Eur. Phys. J. B **2**, 509–523 (1998)

THE EUROPEAN PHYSICAL JOURNAL B

An investigation of the 2D attractive Hubbard model

R. Lacaze[1,2,a], A. Morel[1], B. Petersson[3], and J. Schröper[3]

[1] Service de Physique Théorique, CEA-Saclay, 91191 Gif-sur-Yvette Cedex, France
[2] ASCI, Bâtiment 506, Université Paris Sud, 91405 Orsay Cedex, France
[3] Fakultät für Physik, Universität Bielefeld, Postfach 10 01 31, 33501 Bielefeld, Germany

Received: 30 October 1996 / Revised: 23 October 1997 / Accepted: 29 January 1998

Abstract. We present an investigation of the 2D attractive Hubbard model, considered as an effective model relevant to superconductivity in strongly interacting electron systems. We use both hybrid Monte-Carlo simulations and existing hopping parameter expansions to explore the low temperature domain. The increase of the static S-wave pair correlation with decreasing temperature, which depends weakly on the band filling in the explored temperature range, is analyzed in terms of an expected Kosterlitz-Thouless superconducting transition. Using both our data and previously published results, we show that the evidence for this transition is weak: If it exists, its temperature is very low. The number of unpaired electrons remains nearly constant with temperature at fixed attractive potential strength. In contrast, the static magnetic susceptibility decreases fast with temperature, and cannot be related only to pair formation. We introduce a method by which the Padé approximants of the existing series for the susceptibility give sensible results down to rather low temperature region, as shown by comparison with our numerical data.

PACS. 71.10.Fd Lattice fermion models (Hubbard model, etc.) – 74.25.Dw Superconductivity phase diagrams – 75.40.Mg Numerical simulation studies

1 Introduction

The study of models of strongly interacting electrons is very important for the understanding of high temperature superconductivity. The fundamental mechanism of this phenomenon has not yet been clearly identified, and it may be interesting to study effective models, which have strong local attraction between the electrons. The two dimensional attractive Hubbard [1] model is an example of such a model whose phase diagram as well as physical properties in the normal non superconducting phase can be compared to properties of actual superconducting materials of the high T_c superconductivity class.

The two dimensional attractive Hubbard model is a conceptually simple model, which at low temperatures is expected to have a Kosterlitz-Thouless transition [2] into a superconducting phase, away from half filling. At half filling the model has further symmetries, which prevents such a transition. In the absence of magnetic field, the properties of the model depend on two parameters (apart from the temperature) namely the coupling constant of the attractive local interaction U and the chemical potential μ, measured in units of the coefficient k of the hopping term. The model is solvable in the free case $U = 0$ and the atomic limit $k = 0$. In the interesting case where both U and k are different from zero the model can only be studied through developments around the two solvable cases, high temperature series and numerical simulation techniques. In contrast to the repulsive Hubbard model, with the opposite sign of U, the total fermionic determinant (square of a determinant) is non-negative also for a chemical potential different from zero. Thus the numerical simulations do not suffer from the sign problem in this case. In fact, the two models are related by a change of sign in U and the exchange of chemical potential and magnetic field.

In this paper, using a hybrid Monte-Carlo algorithm, we perform a detailed numerical study of the model in a wide range of values of the parameters. The purpose is first to examine in detail the evidence for a Kosterlitz-Thouless transition and, if it takes place, to estimate the critical temperature. This can be done by studying the s-wave pair-field correlation function, which should diverge at the transition on an infinite lattice. Another interesting quantity is the magnetic susceptibility, sensitive to the presence of single electrons as contrast to those bound in pairs. One may expect the susceptibility to disappear in the strong coupling limit, where more and more pairs are formed. However, at fixed U the temperature behavior of the probability that a site has a single electron and the behavior of the susceptibility are not the same. Therefore the behavior in temperature of the susceptibility of the remnant unpaired electrons is interesting to investigate. For this latter quantity we make use of the series expansion in k given in reference [3], and with the help of the Padé approximants method, extrapolate the series to low

[a] e-mail: lacaze@spht.saclay.cea.fr

temperatures. We compare the results with our numerical data and show that, at least at small and intermediate couplings, rather low temperature may be reached analytically. If true also in the repulsive case of the Hubbard model, where numerical simulations suffer from the sign problem, series expansion might be interesting to use. Unfortunately, no such series are available for the pair field correlator.

There have been some earlier numerical investigations of the same model [4,5], and we compare our results with theirs. Some quantitative discrepancies appear in the results for the pairing correlation, but our main conclusion on a possible KT transition is insensitive to them. In accordance with the independence of the data on filling, already observed [5,6] in the temperature range we study ($T/k > 1/6$ for $U = 4$), no positive evidence for a KT transition away from $1/2$ filling is found from this domain. Investigating the finite size behaviour of the lowest T data of [5] away from $1/2$ filling, not used in this reference, we show that the $T/k = 0.1$ data favour a KT transition, but that if it exists, its temperature can at most reach $\sim$0.04, at variance with the proposed value $T_{KT}/k \sim 0.1$ [5].

In Section 2 we define the model, the observables which we measure and the path integral formalism used for the numerical simulation. In Section 3 we discuss the algorithm employed, which we have chosen as the Hybrid Monte-Carlo algorithm. In Section 4 we discuss our data on the pair field correlation, which is a direct indicator of a transition into a superconducting phase. In Section 5 we present results for the susceptibility, comparing our numerical results with analytic results extrapolated from the series expansion. Section 6, finally, contains a summary and our conclusions.

2 The model

The model is defined by the Hubbard Hamiltonian

$$\begin{aligned} H = & -k \sum_{\langle x,y \rangle} \left(a_x^\dagger a_y + a_y^\dagger a_x + b_x^\dagger b_y + b_y^\dagger b_x \right) \\ & - U \sum_x \left(a_x^\dagger a_x - \frac{1}{2} \right) \left(b_x^\dagger b_x - \frac{1}{2} \right) \\ & - \mu \sum_x \left(a_x^\dagger a_x + b_x^\dagger b_x \right), \end{aligned} \tag{1}$$

where x and y are sites on a two dimensional $N_s \times N_s$ square lattice with $V = N_s^2$ sites, a_x and b_x are coordinate space annihilation operators for spin-up and spin-down electrons respectively, and k is the nearest neighbor hopping parameter. The coupling $U > 0$ denotes the strength of the attractive local interaction and μ is the chemical potential, defined so that $\mu = 0$ at half filling, *i.e.* where the total particle number $\langle N \rangle = V$. Here

$$N = \sum_x (a_x^\dagger a_x + b_x^\dagger b_x). \tag{2}$$

We also define the particle number density operator

$$n = \frac{1}{V} N. \tag{3}$$

The thermodynamics of the model is given by the partition function

$$Z = Tr \left(e^{-\beta H} \right). \tag{4}$$

In the simulation we will measure average values of operators in this ensemble,

$$\langle O \rangle = Tr(O e^{-\beta H})/Z. \tag{5}$$

The basic equal time correlation functions, which give information about the properties of the model are the S-wave on site pairing correlation function

$$P(x-y) = \left\langle (a_x^\dagger b_x^\dagger + b_x a_x)(a_y^\dagger \, b_y^\dagger + b_y a_y) \right\rangle, \tag{6}$$

the correlation function for the magnetization density in the z-direction, or magnetic susceptibility

$$\chi(x-y) = \beta \left\langle (a_x^\dagger a_x - b_x^\dagger b_x)(a_y^\dagger a_y - b_y^\dagger b_y) \right\rangle, \tag{7}$$

and the charge density correlation function

$$C(x-y) = \left\langle (a_x^\dagger a_x + b_x^\dagger b_x)(a_y^\dagger a_y + b_y^\dagger b_y) \right\rangle. \tag{8}$$

The probability that a site is singly occupied is

$$S_1 = \frac{\chi(0)}{\beta}. \tag{9}$$

Furthermore

$$P(0) = 1 - S_1 \tag{10}$$

is the probability of zero or double occupancy.

The correlation function in Fourier space of the quantity E denoted by $\widetilde{E}$ is defined as

$$\widetilde{E}(q) = \sum_z e^{iqz} E(z). \tag{11}$$

An indicator of the diverging correlation length at the phase transition, which has been used *e.g.* in [4,5] is

$$\widetilde{P}_0 \equiv \widetilde{P}\left(q = (0,0)\right). \tag{12}$$

In the same way, the charge density wave indicator is $\widetilde{C}(\pi,\pi)$ and the uniform spin susceptibility is given by $\widetilde{\chi}(0,0)$.

In absence of a magnetic field h the model is invariant under SU(2) spin. For $\mu = h = 0$ it is also invariant under another SU(2) group [7]. This leads to the relation

$$P(z) = (-)^z \left[C(z) - 1 \right]. \tag{13}$$

at $\mu = h = 0$.

As described in the next section, our simulation is based on the Hybrid Monte-Carlo algorithm [8–13].

We thus need the partition function (4) under the form of a path integral where the Hubbard Stratonovich decomposition of the interaction is performed *via* real continuous scalar variables, denoted $\sigma_{x,t}$, where x labels the lattice sites and t the time slices, $t = 1, 2, \cdots N_t$. Up to an irrelevant numerical factor, we get

$$Z = \int \prod_{x,t} [d\sigma_{x,t}]\, e^{-\frac{1}{2}\sum_{x,t}\sigma_{x,t}^2} \times \int \prod_{x,t} [d\eta_{x,t} d\bar{\eta}_{x,t}] \prod_{x,t} \left[d\theta_{x,t} d\bar{\theta}_{x,t}\right] \times \exp\left[\bar{\eta} M \eta + \bar{\theta} M \theta\right]. \quad (14)$$

The Grassmann variables $[\bar{\eta}, \eta]_{x,t}$ (resp. $[\bar{\theta}, \theta]_{x,t}$) are associated with the creation and annihilation operators for the spin up (resp.spin down) electron at site x in time slice t. The fermion matrix is

$$M_{x,t;x',t'} = -\delta_{t-1,t'}\delta_{x,x'} + \delta_{t,t'}\Bigg\{\delta_{x,x'}\mathcal{E}(x,t) + \frac{k\beta}{2N_t}\sum_{\hat{\nu}=\hat{1}}^{\hat{2}}(\delta_{x',x+\hat{\nu}} + \delta_{x',x-\hat{\nu}})\Big\{\mathcal{E}(x,t) + \mathcal{E}(x',t)\Big\} + \frac{k^2\beta^2}{2N_t^2}\sum_{\hat{\nu},\hat{\nu}'=\hat{1}}^{\hat{2}}[\delta_{x',x+\hat{\nu}+\hat{\nu}'} + \delta_{x',x-\hat{\nu}-\hat{\nu}'} + 2\delta_{x',x+\hat{\nu}-\hat{\nu}'}]\Bigg\}, \quad (15)$$

where $\mathcal{E}(x,t)$ is defined as

$$\mathcal{E}(x,t) = \exp\left[\sqrt{\frac{U\beta}{N_t}}\sigma_{x,t} - (U-\mu)\frac{\beta}{N_t}\right].$$

The two equations (14) and (15) follow from a standard Trotter decomposition. The kinetic part K and the interaction part V of the Hamiltonian appear in each time slice as

$$\exp(-\frac{\beta}{N_t}K) \times \exp(-\frac{\beta}{N_t}V),$$

which is known to reproduce Z and averages like equation (5) up to corrections of order $1/N_t^2$ (precise statements and references to earlier work can be found in [14]). We expanded the kinetic factor in powers of β/N_t, keeping only terms relevant at this order, which yields the matrix M as a sparse matrix, hence saving some computer time. The same goal can be reached by a checkerboard breakup of the kinetic term (see *e.g.* [15]). In the latter case, particle-hole symmetry is exactly respected, while here it is broken by terms of order $1/N_t^2$. As we will see in the next section, we take advantage of this feature by using $\langle n\rangle - 1$ at zero chemical potential as an indicator of how large typical $\mathcal{O}(1/N_t^2)$ terms may be. As another check that the values of N_t used are large enough, we also estimated the effect of further truncating the expansion of the kinetic term, replacing M equation (15) by $M_{(1)}$, where

$$M_{(1)x,t;x',t'} = \frac{k\beta}{N_t}\delta_{t,t'}\sum_{\hat{\nu}=\hat{1}}^{\hat{2}}(\delta_{x',x+\hat{\nu}} + \delta_{x',x-\hat{\nu}}) - \delta_{x,x'}\delta_{t-1,t'} + \delta_{x,x'}\delta_{t,t'}\exp\left[\sqrt{\frac{U\beta}{N_t}}\sigma_{x,t} - (U-\mu)\frac{\beta}{N_t}\right]. \quad (16)$$

Using $M_{(1)}$ we expect corrections of order $1/N_t$.

The integrals over the Grassmann variables may be performed, and from equations (14–15) we get

$$Z = \int \prod_{x,t} [d\sigma_{x,t}]\, e^{-\frac{1}{2}\sum_{x,t}\sigma_{x,t}^2} \left(\det M\right)^2. \quad (17)$$

As $\det M = \left(\det M^\dagger\right)$ one has $\left(\det M\right)^2 = \det\left(M^\dagger M\right)$, which is useful for the construction of the algorithm.

For the observables of interest, listed in equations (3, 6–8), the following expressions follow in the absence of a magnetic field (explicit use of the up-down spin symmetry has been made).

$$\langle n\rangle = 2 - 2\langle M^{-1}_{x,N_t;x,1}\rangle, \quad (18)$$

$$P(x-y) = \delta_{xy}\left[1 - 2\left\langle M^{-1}_{x,N_t;x,1}\right\rangle\right] + 2\left\langle\left(M^{-1}_{x,N_t;y,1}\right)^2\right\rangle, \quad (19)$$

$$\frac{\chi(x-y)}{\beta} = 2\delta_{xy}\langle M^{-1}_{x,N_t;x,1}\rangle - 2\langle M^{-1}_{x,N_t;y,1}M^{-1}_{y,N_t;x,1}\rangle, \quad (20)$$

$$C(x-y) = 2\delta_{xy}\left\langle M^{-1}_{x,N_t;x,1}\right\rangle + 4 - 8\left\langle M^{-1}_{x,N_t;x,1}\right\rangle + 4\left\langle M^{-1}_{x,N_t;x,1}M^{-1}_{y,N_t;y,1}\right\rangle - 2\left\langle M^{-1}_{x,N_t;y,1}M^{-1}_{y,N_t;x,1}\right\rangle. \quad (21)$$

Note the time labels (N_t,1), rather than, say, (1,1), appearing in the matrix elements associated with operators all taken at the same time $t = 1$. In deriving these expressions, we closely followed Creutz [11]. In particular, his analysis shows that while one would expect $\langle M^{-1}_{x,1;x,1}\rangle$ for $\langle n/2\rangle$, equation (18) is the correct expression to use in order not to spoil the order $1/N_t^2$ accuracy which is looked for. We actually verified that at zero chemical potential, the estimate (18) gives an answer much closer to $\langle n\rangle = 1$ than the other one.

We will also consider the average value of the field σ'_x defined as

$$\sigma'_{x,t} = \sqrt{\frac{N_t}{\beta}}\sigma_{x,t}. \quad (22)$$

Indeed, from the equation of motion for the σ-fields, which can easily be derived from equation (14), we have

$$\lim_{N_t\to\infty} \langle \sigma'_{x,t} \rangle = \sqrt{U}\, \langle n \rangle \,. \tag{23}$$

This relation will be also used as a check that we actually considered large enough N_t values.

3 The numerical simulation

The expectation values of (18-22) are obtained from σ-field configurations corresponding to the partition function (17). These configurations are generated with an Hybrid Monte-Carlo algorithm (HMC-algorithm) which is a widely used tool to simulate systems involving fermions (*e.g.* [8–13]). Its main virtues are that it is an exact algorithm and that, at least in principle, the computer time grows slowly with system size.

Introducing one set of pseudofermion fields $\phi^{(i)}$ for each species η and θ and momenta p conjugate to the σ fields, the Hamiltonian of the system can be written as

$$\mathcal{H} = \frac{1}{2}\sum_j p_j^2 + \frac{1}{2}\sum_j \sigma_j^2 + \sum_{i=1}^{2}\sum_{j,k} \phi_j^{(i)} \left(M^\dagger M\right)^{-1}_{jk} \phi_k^{(i)}, \tag{24}$$

where j and k denote sites on the $N_s^2 \times N_t$ lattice. Starting from a configuration σ, a new configuration is obtained in three steps.

i) First the pseudofermion fields are generated from Gaussian distributed vectors $r^{(i)}$ by $\phi^{(i)} = M^\dagger(\sigma) r^{(i)}$ and Gaussian momenta p are chosen.

ii) Then σ and p are updated by molecular dynamics with $\mathcal{H}$ as Hamiltonian, the set of Hamilton's equations being solved with a discrete time step $d\tau$. So $\mathcal{H}$ is a constant of motion in the limit $d\tau \to 0$. The integration of the molecular dynamics equation is performed by a leapfrog method [12]

$$\sigma_j|_{(n+1)d\tau} = \sigma_j|_{nd\tau} + d\tau\; p_j - \frac{(d\tau)^2}{2}\left.\frac{\partial \mathcal{H}}{\partial \sigma_j}\right|_{nd\tau}, \tag{25}$$

$$p_j|_{(n+1)d\tau} = p_j|_{nd\tau} - \frac{d\tau}{2}\left(\left.\frac{\partial \mathcal{H}}{\partial \sigma_j}\right|_{nd\tau} + \left.\frac{\partial \mathcal{H}}{\partial \sigma_j}\right|_{(n+1)d\tau}\right). \tag{26}$$

iii) After n_{MD} steps, the move to the resulting σ configuration is accepted or refused by a Metropolis test. In both cases, one restarts at step i) with either the accepted configuration or the old one respectively.

This algorithm introduces two parameters, the number of steps n_{MD} and the step size $d\tau$. The correlation between configurations decreases when the trajectory length $\tau = n_{MD} d\tau$ increases, while increasing n_{MD} increases the computation time and increasing $d\tau$ decreases the acceptance. We have taken $\tau \sim 1.0$, (more precisely between 0.8 and 1.6) with n_{MD} such that a large enough acceptance is reached for all the volumes used (the acceptance decreases with increasing volume [11,12]). This is obtained with $n_{MD} \sim 4\beta U$. We also tested trajectories with Poisson-distributed lengths, *i.e.* n_{MD} distributed around a certain mean value and $d\tau$ held fixed [16,17]. This does not decorrelate measurements of observables compared to τ fixed. The only effect is to increase the acceptance by a few percent if n_{MD} is small.

For an observable O whose value at Monte-Carlo time i is O_i the autocorrelation function is

$$C_O(t) = \frac{\langle O_i O_{i+t}\rangle - \langle O_i\rangle^2}{\langle O_i^2\rangle - \langle O_i\rangle^2}, \tag{27}$$

where $\langle\ \rangle$ means the average over Monte-Carlo time i. We estimated the autocorrelation time ξ_O by

$$\xi_O = \frac{1}{t_c}\sum_0^{t_c-1} \ln\left[\frac{C_O(t)}{C_O(t+1)}\right], \tag{28}$$

disregarding the noisy region $t > t_c$ where t_c is the smallest t value such that $C_O(t)$ is less than 0.05. This gives the exact autocorrelation time if C_O is purely exponential. The integrated autocorrelation time

$$t_{int} = \sum_0^{t_c-1} C_O(t), \tag{29}$$

coincides with ξ_O within 5% under the same assumption.

The physical and algorithmic parameters are given in Tables 1 and 2 along with the number of trajectories simulated, the autocorrelation time $\xi_{\sigma'}$ and the acceptance. Here $\xi_{\sigma'}$ denotes the autocorrelation length for the *lattice average* of the σ' field. It is computed automatically and may be occasionally overestimated due to large noise to signal ratio around $t = t_c$. It is found quite large, in fact much larger by at least one order of magnitude than those measured for the observables built from the inverse fermion matrix equations (18−21). Because any measurement of physical quantities is uniquely determined by the data of a particular σ configuration, we conservatively consider $\xi_{\sigma'}$ as a safe scale to appreciate the length of MC runs while keeping the other autocorrelation times for error estimating (we do not know what QMC simulations obtain for the analogous quantity, with the σ fields replaced by Ising variables, expressed in number of sweeps through the lattice).

The updates of σ_j and p_j (Eqs. (25, 26)) require twice the computation of a vector $u = \left(M^\dagger M\right)^{-1}\phi$ for a given ϕ. This computation, which costs most of the computer time, is performed by a conjugate gradient subroutine with a diagonal preconditioning [18], which speeds up the convergence considerably. The conjugate gradient iteration is stopped after c_{cg} steps, when the iterative rest $r^2_{c_{cg}}$ becomes less than $10^{-10}|\phi|^2$.

The number c_{cg} of conjugate-gradient iterations can be significantly reduced if we use for u_0 the value obtained

Table 1. Parameters of the simulations performed at $U = 4$. Also given are the number of trajectories generated, the σ' field autocorrelation time $\xi_{\sigma'}$ and the acceptance.

Lattice	U	β	$-\mu$	τ	n_{MD}	Traj.	$\xi_{\sigma'}$	Acc.
$4^2\times16$	4	1	0.15	1.6	16	19270	37	0.99
$4^2\times8$	4	1	0.15	1.6	16	20000	23	0.99
$6^2\times8$	4	1	0.15	1.6	16	20000	21	0.98
$4^2\times16$	4	1	0.0	1.6	16	19160	38	0.99
$4^2\times8$	4	1	0.0	1.6	16	20000	23	0.99
$6^2\times16$	4	1	0.0	1.6	16	20000	36	0.98
$6^2\times8$	4	1	0.0	1.6	16	20000	22	0.98
$4^2\times16$	4	2	0.15	1.6	32	12500	33	0.98
$4^2\times16$	4	2	0.0	1.6	32	12500	33	0.98
$4^2\times24$	4	3	0.15	1.6	48	12250	81	0.95
$4^2\times24$	4	3	0.0	1.6	48	12500	54	0.95
$4^2\times32$	4	4	0.6	0.8	64	22500	91	0.99
$4^2\times32$	4	4	0.45	0.8	64	22210	191	0.99
$6^2\times32$	4	4	0.45	1.6	64	20970	43	0.85
$6^2\times32$	4	4	0.2	1.6	64	43340	158	0.83
$4^2\times32$	4	4	0.15	0.8	64	19800	290	0.98
$6^2\times32$	4	4	0.15	1.6	64	20220	67	0.82
$8^2\times32$	4	4	0.15	1.6	64	18490	126	0.71
$6^2\times32$	4	4	0.1	1.6	64	20530	50	0.82
$4^2\times32$	4	4	0.0	0.8	64	19960	228	0.98
$4^2\times64$	4	4	0.0	1.6	64	20000	121	0.94
$6^2\times32$	4	4	0.0	1.6	64	20270	82	0.84
$4^2\times64$	4	6	0.45	1.2	96	10000	127	0.98
$6^2\times64$	4	6	0.45	1.2	96	9200	109	0.88
$4^2\times64$	4	6	0.3	1.2	96	12500	292	0.96
$6^2\times64$	4	6	0.3	1.2	96	12500	146	0.87
$6^2\times64$	4	6	0.23	1.2	96	12500	170	0.85
$4^2\times64$	4	6	0.15	1.2	96	19300	335	0.96
$6^2\times64$	4	6	0.15	1.2	96	12500	565	0.85
$8^2\times64$	4	6	0.15	1.2	96	8200	250	0.64
$4^2\times64$	4	6	0.08	1.2	96	20000	743	0.96
$4^2\times64$	4	6	0.0	1.2	96	12500	185	0.97
$6^2\times64$	4	6	0.0	1.2	96	10000	179	0.85

Table 2. Parameters of the simulations performed at $U = 2$ and 8. Also given are the number of trajectories generated, the σ' field autocorrelation time $\xi_{\sigma'}$ and the acceptance.

Lattice	U	β	$-\mu$	τ	n_{MD}	Traj.	$\xi_{\sigma'}$	Acc.
$4^2\times8$	2	1	0.0	1.6	8	20000	13	0.98
$4^2\times16$	2	2	0.0	1.6	16	9230	15	0.98
$6^2\times32$	2	4	0.15	1.6	32	16140	18	0.96
$6^2\times16$	2	4	0.15	1.6	32	47000	13	0.90
$6^2\times32$	2	4	0.0	1.6	32	47180	20	0.96
$6^2\times16$	2	4	0.0	1.6	32	38000	13	0.90
$6^2\times24$	2	6	0.3	1.6	48	17780	13	0.84
$6^2\times24$	2	6	0.15	1.6	48	16810	28	0.79
$6^2\times24$	2	6	0.0	1.6	48	23420	24	0.77
$6^2\times32$	8	0.5	0.15	1.6	16	20700	240	0.99
$6^2\times32$	8	0.5	0.0	1.6	16	20500	162	0.99
$6^2\times32$	8	2.0	0.15	1.6	64	12612	1237	0.95
$6^2\times32$	8	2.0	0.0	1.6	64	18855	782	0.94

at the previous molecular dynamics step. However this method leads to a decrease of the acceptance when increasing β and V, associated with uncontrolled biases. So we always start with $u_0 = 0$, in such a way that no peculiar direction of phase space is favored or suppressed by the rounding off errors.

The value of c_{cg} needed to reach the prescribed accuracy ranges between $\sim 30\%$ and $\sim 65\%$ of the vector length. However in some cases, this accuracy is not obtained in $N_s^2 \times N_t$ iterations, in particular for small volumes. Such situations can be avoided by reducing the trajectory length τ, and this explains the values $\tau = 0.8$ and 1.2 in Table 1. Of course, this comes with the price of increasing the σ autocorrelation times.

The above behaviours of c_{cg} apparently contradict those reported in [10], where the dependences on the parameters N_s^2, U and β are found very weak. In fact, we can obtain similar performances, although using poorer preconditioning, by replacing our stopping criterion $r^2_{c_{cg}} < 10^{-10}|\phi|^2$ by the less demanding $r^2_{c_{cg}} < 4 \times 10^{-6}$ V set in [10]. This we understand as follows. As a function of the number n of iterations, the rest r_n^2 generically exhibits two successive regimes. The first is rather slow, until n reaches a crossover value n_{cr}, beyond which fast convergence shows up. We observe that most of the dependence on the parameters resides in that of n_{cr}. Thus if the stopping criterion is chosen *above* $r^2_{n_{cr}}$, c_{cg} remains roughly parameter independent, while achieving true convergence requires reaching n_{cr}, which is more and more costly.

In order to keep control on the effect of finite N_t values, we first compared results obtained with different N_t both with the matrix M of equation (15) and its truncated form $M_{(1)}$, equation (16). Table 3 shows some of these data, taken at $\mu = 0$, $U = 4$ on a 4^2 lattice. In agreement with the expectations discussed in Section 3, we do observe that $\langle\sigma'\rangle$ and $\langle n\rangle$ approach their exact asymptotic values 2 and 1 respectively, at a rate compatible with $\mathrm{O}(1/N_t)$ when $M_{(1)}$ is used, while M already provides good answers in the same N_t ranges. The pairing $\widetilde{P}_0$ is less sensitive to these various changes. This is not so for the susceptibility, which increases substantially with N_t. We attribute this sensitivity to the occurrence of important cancellations in building up $\widetilde{\chi}$, between a large positive contribution of $\chi(x - y = 0)$ and the sum of negative contributions from $\chi(x - y \neq 0)$.

Because increasing N_t is costly in computer time, we used $N_t = 2\beta U$. Exceptions concern the case $\beta = 0.5$, $U = 8$ ($N_t = 32$) and the low temperature points $\beta = 6$, $U = 4$ ($N_t = 64$). In order to verify that these values of N_t are large enough, we made further runs with higher N_t values at $U = 4$. The comparison is summarized in Table 4.

The results for different N_t values are in general agreement with each other. However, differences well outside the errors quoted appear for $\widetilde{\chi}$ and S_1, which both increase with N_t. With an approach to asymptotics expected of

Table 3. Comparison of data taken with the fermionic matrix to order 1 and 2 in $1/N_t$. See equations (16, 15) respectively.

Lattice	U	β	μ	order	$\langle\sigma'\rangle$	$\langle n\rangle/2$	$\widetilde{P}_0$	$\widetilde{\chi}\times 10$
$4^2\times 16$	4	1	0.0	1	1.76(1)	0.468(2)	1.060(2)	1.406(3)
$4^2\times 48$	4	1	0.0	1	1.94(2)	0.492(4)	1.060(3)	1.398(3)
$4^2\times 8$	4	1	0.0	2	2.05(2)	0.501(4)	1.071(4)	1.301(8)
$4^2\times 16$	4	1	0.0	2	1.96(3)	0.490(5)	1.062(5)	1.390(9)
$4^2\times 32$	4	4	0.0	1	1.34(2)	0.401(3)	2.20(3)	0.81(1)
$4^2\times 64$	4	4	0.0	1	1.66(3)	0.451(6)	2.27(6)	0.79(2)
$4^2\times 32$	4	4	0.0	2	2.11(4)	0.514(4)	2.37(9)	0.51(2)
$4^2\times 64$	4	4	0.0	2	1.98(3)	0.495(5)	2.55(9)	0.71(2)

Table 4. Comparison of data taken at different N_t values.

Lattice	U	β	$-\mu$	$\langle\sigma'\rangle$	$\langle n\rangle/2$	$\widetilde{P}_0$	$\widetilde{\chi}\times 10$	S_1
$4^2\times 16$	4	1	0.15	1.81(3)	0.453(5)	1.062(5)	1.379(9)	0.264(2)
$4^2\times 8$	4	1	0.15	1.90(2)	0.463(4)	1.072(4)	1.289(8)	0.250(2)
$4^2\times 16$	4	1	0.0	1.96(3)	0.490(5)	1.062(5)	1.390(9)	0.266(2)
$4^2\times 8$	4	1	0.0	2.05(2)	0.501(4)	1.071(4)	1.301(8)	0.252(2)
$6^2\times 16$	4	1	0.0	2.02(2)	0.501(3)	1.072(7)	1.382(8)	0.267(1)
$6^2\times 8$	4	1	0.0	2.03(2)	0.496(3)	1.075(6)	1.313(8)	0.255(1)
$4^2\times 64$	4	4	0.0	1.98(3)	0.495(5)	2.55(9)	0.71(2)	0.244(2)
$4^2\times 32$	4	4	0.0	2.11(4)	0.514(4)	2.37(9)	0.51(2)	0.230(4)
$6^2\times 96$	4	6	0.0	2.04(4)	0.505(1)	3.2(2)	0.37(3)	0.251(5)
$6^2\times 64$	4	6	0.0	2.01(3)	0.493(2)	3.8(2)	0.36(3)	0.235(4)

order $(\beta/N_t)^2$ this does not affect the physical discussion given below. No general trend can be deduced from these data for $\widetilde{P}_0$. We cannot exclude that the choice $N_t = 2\beta U$, although it seems to be the standard one in similar investigations, is not large enough. Warnings about possible pathologies at low temperatures for certain correlation functions have been addressed by Fye and Scalettar [16] and one may find references to observed anomalies therein. Note that at $\beta = 6, U = 4$, we used more conservative values.

The results obtained for $\langle\sigma'\rangle$, filling of the band $\langle n\rangle/2$, pairing correlation $\widetilde{P}_0$, spin susceptibility $\widetilde{\chi}$ and single occupation probability S_1 for various lattices and values of the inverse temperature β and chemical potential μ are given in Tables 5 and 6. The errors reported therein are calculated by incorporating the autocorrelation time t_{int} of equation (29) by using a variance which is the naive variance multiplied by $(1 + 2t_{int})$.

Comparing our results for $\widetilde{P}_0$ at $U = 4$ (Tab. 5) with those of [5] shows the existence of some discrepancy at low temperature, especially at $\beta = 6$. This is discussed in the next section, where in particular a more refined analysis of the numerical output is presented.

4 The S-wave pair-field correlation function

One of the observables of interest in the context of a superconducting phase transition is the pairing correlation function P and its Fourier transform $\widetilde{P}$. They are defined by (6) and (11) respectively. In the present work we have studied the $q = (0, 0)$ equal-time s-wave pair-field correlation function $\widetilde{P}_0$, equation (12), which has previously been examined *e.g.* in [4,5]. For this quantity we obtain from equation (19)

$$\widetilde{P}_0 = 1 - 2\left\langle M^{-1}_{x,N_t;x,1}\right\rangle + 2\sum_y \left\langle \left(M^{-1}_{y,N_t;x,1}\right)^2\right\rangle. \quad (30)$$

We first discuss the expected behaviour of $\widetilde{P}_0$, then comment on peculiar features encountered in data analysis, and finally present our interpretation of the results, comparing them with previous works.

4.1 Expected dependences on μ, T, U and N_s

Let us recall [4,5] what can be expected on general grounds for the behavior of $\widetilde{P}_0$ as a function of β, U, μ and N_s, the linear size of the lattice.

A first remark is that under a global particle-hole transformation

$$a_x \to (-)^x a^\dagger_x \quad (31)$$

$$b_x \to (-)^x b^\dagger_x \quad (32)$$

which changes $H(\mu)$ of equation (1) into $H(-\mu)$, up to an irrelevant additive constant, the operator defining P in

Table 5. Data obtained on various lattices at $U = 4$: $\langle\sigma'\rangle$, filling of the band $\langle n\rangle/2$, pairing correlation $\widetilde{P}_0$, spin susceptibility $\widetilde{\chi}$ and single occupation probability S_1 for different values of the inverse temperature and of the chemical potential.

Lattice	U	β	$-\mu$	$\langle\sigma'\rangle$	$\langle n\rangle/2$	$\widetilde{P}_0$	$\widetilde{\chi}\times 10$	S_1
$4^2\times 8$	4	1	0.15	1.90(2)	0.463(4)	1.072(4)	1.289(8)	0.250(2)
$4^2\times 8$	4	1	0.0	2.05(2)	0.501(4)	1.071(4)	1.301(8)	0.252(2)
$6^2\times 8$	4	1	0.15	1.91(1)	0.463(2)	1.079(7)	1.300(8)	0.253(1)
$6^2\times 8$	4	1	0.0	2.03(2)	0.496(3)	1.075(6)	1.313(8)	0.255(1)
$4^2\times 16$	4	2	0.15	1.81(3)	0.440(5)	1.64(2)	1.16(2)	0.240(2)
$4^2\times 16$	4	2	0.0	2.02(3)	0.494(4)	1.63(3)	1.18(2)	0.244(2)
$4^2\times 24$	4	3	0.15	1.81(3)	0.435(3)	2.18(5)	0.85(3)	0.234(2)
$4^2\times 24$	4	3	0.0	2.10(3)	0.509(6)	2.23(5)	0.87(2)	0.242(2)
$4^2\times 32$	4	4	0.6	1.31(2)	0.309(1)	2.47(7)	0.45(2)	0.226(4)
$4^2\times 32$	4	4	0.45	1.40(3)	0.335(2)	2.6(1)	0.46(2)	0.234(1)
$4^2\times 32$	4	4	0.15	1.87(6)	0.45(1)	2.40(6)	0.55(2)	0.234(4)
$4^2\times 32$	4	4	0.0	2.11(4)	0.514(4)	2.37(9)	0.51(2)	0.230(4)
$6^2\times 32$	4	4	0.45	1.38(1)	0.329(1)	3.0(1)	0.72(1)	0.226(1)
$6^2\times 32$	4	4	0.2	1.74(2)	0.422(2)	2.87(5)	0.697(9)	0.234(1)
$6^2\times 32$	4	4	0.15	1.83(2)	0.443(2)	3.1(1)	0.68(1)	0.232(2)
$6^2\times 32$	4	4	0.1	1.92(1)	0.468(2)	3.1(2)	0.71(1)	0.234(1)
$6^2\times 32$	4	4	0.0	2.06(2)	0.501(3)	3.05(9)	0.75(1)	0.239(1)
$8^2\times 32$	4	4	0.15	1.86(2)	0.449(2)	2.85(8)	0.72(1)	
$4^2\times 64$	4	6	0.45	1.31(3)	0.321(2)	2.38(8)	0.14(2)	0.246(6)
$4^2\times 64$	4	6	0.3	1.41(4)	0.344(2)	2.9(1)	0.22(2)	0.242(6)
$4^2\times 64$	4	6	0.15	1.61(4)	0.396(3)	3.3(2)	0.23(2)	0.234(4)
$4^2\times 64$	4	6	0.08	1.86(6)	0.460(7)	2.58(9)	0.18(1)	0.222(4)
$4^2\times 64$	4	6	0.0	2.03(4)	0.503(7)	2.57(9)	0.17(2)	0.236(6)
$6^2\times 64$	4	6	0.45	1.32(2)	0.322(2)	4.0(3)	0.38(3)	0.224(6)
$6^2\times 64$	4	6	0.3	1.46(2)	0.359(1)	4.2(2)	0.37(4)	0.240(4)
$6^2\times 64$	4	6	0.23	1.62(2)	0.396(1)	4.2(2)	0.42(2)	0.244(4)
$6^2\times 64$	4	6	0.15	1.83(5)	0.452(2)	3.9(3)	0.31(2)	0.238(4)
$6^2\times 64$	4	6	0.0	2.01(2)	0.493(2)	3.8(2)	0.36(3)	0.236(4)
$8^2\times 64$	4	6	0.15	1.75(3)	0.429(1)	4.9(4)	0.49(3)	0.242(2)

Table 6. Data obtained on various lattices at $U = 2$ and 8. As in Table 5.

Lattice	U	β	$-\mu$	$\langle\sigma'\rangle$	$\langle n\rangle/2$	$\widetilde{P}_0$	$\widetilde{\chi}\times 10$	S_1
$4^2\times 8$	2	1	0.0	1.45(1)	0.502(2)	0.886(1)	2.114(4)	0.3738(8)
$4^2\times 16$	2	2	0.0	1.42(2)	0.497(3)	1.127(4)	2.46(1)	0.373(1)
$6^2\times 32$	2	4	0.15	1.268(7)	0.438(1)	1.46(1)	2.55(1)	0.3732(8)
$6^2\times 32$	2	4	0.0	1.453(4)	0.504(1)	1.445(7)	2.727(9)	0.3746(4)
$6^2\times 24$	2	6	0.3	1.153(4)	0.3747(8)	1.99(2)	1.30(2)	0.3446(6)
$6^2\times 24$	2	6	0.15	1.340(8)	0.440(2)	2.20(6)	1.69(2)	0.3444(8)
$6^2\times 24$	2	6	0.0	1.605(6)	0.531(2)	2.10(3)	1.86(2)	0.346(1)
$6^2\times 32$	8	0.5	0.15	2.69(7)	0.475(8)	0.948(3)	0.667(5)	0.174(2)
$6^2\times 32$	8	0.5	0.0	2.88(6)	0.509(8)	0.955(4)	0.661(5)	0.173(2)
$6^2\times 32$	8	2	0.15	2.3(2)	0.41(3)	1.9(1)	0.104(5)	0.079(2)
$6^2\times 32$	8	2	0.0	2.7(1)	0.47(2)	2.2(2)	0.116(5)	0.085(2)

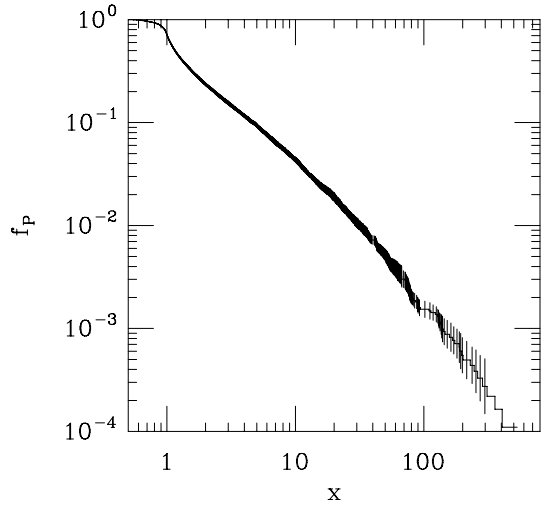

Fig. 1. Fraction of events with $\widetilde{P}_0 > x$ as a function of x for $U = 4$, $\beta = 4$ and $\mu = 0$.

equation (6) remains unchanged. Hence

$$\widetilde{P}_0(\mu) = \widetilde{P}_0(-\mu), \tag{33}$$

whereas the filling density satisfies

$$\langle n \rangle (\mu) = 1 - \langle n \rangle (-\mu). \tag{34}$$

In the vicinity of $\mu = 0$, and above any transition temperature which could lead to non-analyticities, we thus expect $\widetilde{P}_0$ to be a function of μ^2, while $\langle n \rangle (\mu)$ is linear in μ.

At $\mu = 0$, because of the $SU(2)'$ symmetry, no transition may occur at $T \neq 0$, and as $T \to 0$, $\widetilde{P}_0$ and the correlation length ξ are expected to diverge according to

$$\xi \propto \exp(A/T) \tag{35}$$

$$\widetilde{P}_0 = b \exp(a/T) \propto \xi^2. \tag{36}$$

At $\mu \neq 0$, the $SU(2)'$ symmetry is broken down to a $U(1)$ symmetry associated with the particle number, which can lead to a finite T transition of the Kosterlitz-Thouless [2] type. Then the expectation is, above the critical temperature T_{KT},

$$\xi_{KT} \propto \exp\left[A/\sqrt{T - T_{KT}(\mu, U)}\right] \tag{37}$$

and

$$\widetilde{P}_0 = b \exp\left[a/\sqrt{T - T_{KT}(\mu, U)}\right] \propto \xi_{KT}^{2-\eta_{KT}}, \tag{38}$$

with $\eta_{KT} = 0.25$. Of course $a = (2 - \eta_{KT})A$ and b are functions of μ and U. Also T dependent prefactors may occur in these expressions. But it is reasonable to think that the μ,U dependences of ξ_{KT} and $\widetilde{P}_0$ are dominated by that of $T - T_{KT}$.

Table 7. $\widetilde{P}_0$ values obtained at $U = 4$, $\mu = 0$ and $\mu = -0.15$: $\widetilde{P}_0^{stand}$ as in Table 5 and $\widetilde{P}_0^{cor}$ the corrected values according to the analysis of Section 4.2.

Lattice	U	β	$-\mu$	$\widetilde{P}_0^{\rm stand}$	$\widetilde{P}_0^{\rm cor}$	ν
$4^2\times8$	4	1	0.15	1.072(4)	1.073(5)	≥ 1.9
$4^2\times8$	4	1	0.0	1.071(4)	1.072(4)	≥ 1.9
$6^2\times8$	4	1	0.15	1.079(7)	1.080(7)	≥ 1.9
$6^2\times8$	4	1	0.0	1.075(6)	1.078(7)	≥ 1.9
$4^2\times16$	4	2	0.15	1.64(2)	1.64(2)	≥ 1.8
$4^2\times16$	4	2	0.0	1.63(3)	1.63(3)	≥ 1.8
$4^2\times24$	4	3	0.15	2.18(5)	2.21(6)	≥ 1.8
$4^2\times24$	4	3	0.0	2.23(5)	2.24(8)	≥ 1.8
$4^2\times32$	4	4	0.15	2.40(6)	2.5(2)	[1.55-1.75]
$4^2\times32$	4	4	0.0	2.37(9)	2.4(3)	[1.55-1.75]
$6^2\times32$	4	4	0.15	3.1(1)	3.2(2)	[1.55-1.75]
$6^2\times32$	4	4	0.0	3.05(9)	3.2(2)	[1.55-1.75]
$8^2\times32$	4	4	0.15	2.85(8)	2.9(2)	[1.55-1.75]
$4^2\times64$	4	6	0.15	3.3(2)	3.7(4)	[1.25-1.35]
$4^2\times64$	4	6	0.0	2.57(9)	3.1(4)	[1.25-1.35]
$6^2\times64$	4	6	0.15	3.9(3)	4.6(7)	[1.25-1.35]
$6^2\times64$	4	6	0.0	3.8(2)	4.4(6)	[1.25-1.35]
$8^2\times64$	4	6	0.15	4.9(4)	5.8(6)	[1.25-1.35]

In a finite system of size N_s^2, standard scaling arguments predict a behavior

$$\widetilde{P}_{0,N_s} \simeq N_s^2 f(N_s/\xi) \text{ at } \mu = 0, \tag{39}$$

and

$$\widetilde{P}_{0,N_s} \simeq N_s^{2-\eta_{KT}} f(N_s/\xi_{KT}) \text{ at } \mu \neq 0 \tag{40}$$

for the pair correlation, in a domain of parameters β, μ, U where the ξ's are large, and N_s/ξ is kept fixed.

On the basis of numerical QMC simulations of the model, reference [5] confirmed this overall picture and concluded that a maximum transition temperature of order 0.2 is reached for $U \simeq 8$ and $\langle n \rangle \simeq 0.85$, while at $U = 4$ the critical temperature T_{KT} is of order 0.1 and 0.05 respectively at $\langle n \rangle = 0.87$ and 0.5. A study of T_{KT} as a function of U and $\langle n \rangle$ is performed in [19]. There, the helicity modulus is calculated in the BCS framework (an approach which may be questioned when U is not small), and its relationship with the transition temperature in a KT-like transition is exploited. Values of T_{KT} much higher than in [5] are found. After refining our analysis of the numerical data for $\widetilde{P}_0$, we will reexamine the question.

4.2 Observed properties and analysis of our HMC data

The average values and statistical errors given in Tables 5 and 6 were obtained *via* the quite standard methods indicated at the end of Section 3. In these treatments it is implicitly assumed that the distribution f_O of an observable O admits a finite variance $v = \langle O^2 \rangle - \langle O \rangle^2$, so that the

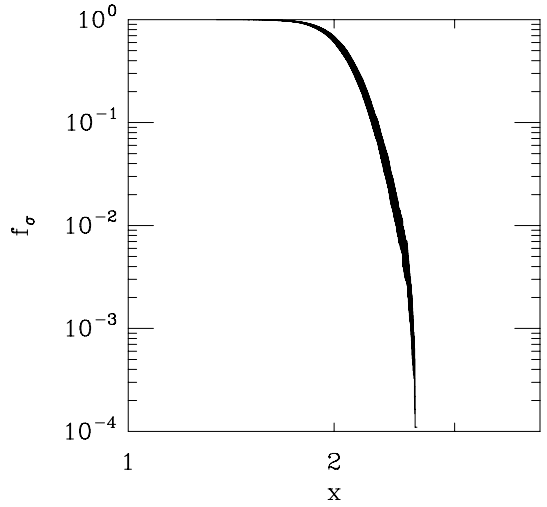

Fig. 2. Fraction of events with $\sigma > x$ as a function of x for $U = 4$, $\beta = 4$ and $\mu = 0$.

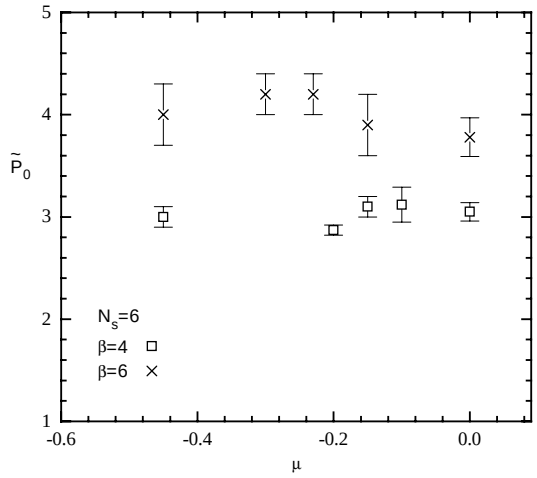

Fig. 3. $\widetilde{P}_0$ as a function of μ for $U = 4$ (values from Tab. 5).

statistical error associated with N independent measurements is $\delta O \sim (v/N)^{1/2}$, in the large N limit. In the case of $\widetilde{P}_0$, especially at low temperature, such a behaviour was not clearly observed, and the existence of a very large tail in the $\widetilde{P}_0$ distribution made us suspicious about the above property being valid. Note that here $\widetilde{P}_0$ is a shorthand notation for the random σ–dependent variable whose expectation value is taken in equation (30). Figure 1 shows the measured probability for finding $\widetilde{P}_0 > x$ in N events on a $6^2 \times 32$ lattice, for $\beta = 4$, $U = 4$ and $\mu = 0$, namely the log-log plot *versus* x of

$$f_P(x) = \frac{1}{N}\big(\#\text{ events with } \widetilde{P}_0 > x\big). \qquad (41)$$

The errors are estimated from the fluctuations observed amongst 10 bins. In contrast with the similar data for σ' shown in Figure 2, where f_σ falls down abruptly above $x = \langle\sigma'\rangle \sim 2$, there is a sizable probability for finding $\widetilde{P}_0 \gg \langle\widetilde{P}_0\rangle$, moreover compatible with

$$f_P(x) = \frac{c}{\nu} x^{-\nu} \qquad \text{at large } x, \quad \text{with } 1 < \nu < 2, \qquad (42)$$

in which case the variance does not exist. The P distribution is said to be in the attraction basin of a Lévy law (see *e.g.* [20] and references therein). In order to appreciate the effect of this behaviour on our estimates of $\widetilde{P}_0$ and of its error, let us now *assume* the distribution f_P to be given by equation (42) for $x > x_c$. Then if K events are observed below x_c, we have that $(N - K)/N = c/\nu x_c^{-\nu}$, which fixes c, given x_c and ν, and gives the estimate

$$\langle\widetilde{P}_0\rangle(x_c) = \frac{1}{N}\sum_{P_i < x_c} P_i \; + \frac{N-K}{N}\frac{\nu}{\nu-1} x_c. \qquad (43)$$

If the assumption (42) is valid and ν properly chosen, the estimate (43) must be independent of x_c provided x_c is large enough and enough events are observed for $x > x_c$. Within our statistics, this requirement was not sufficient to determine ν accurately, but we consistently found a range of ν values for which (43) provides a plateau at large x_c. For ν at the central value of this range, we take the height of the plateau as a corrected estimate $\widetilde{P}_0^{cor}$ of $\widetilde{P}_0$, and associate an error, which includes the statistical jackknife error and the effect of varying ν within the accepted range.

For $U = 4$, $\mu = 0.0$ and -0.15, and various lattice sizes, $\widetilde{P}_0^{cor}$ is compared in Table 7 with $\widetilde{P}_0^{stand}$, the estimate previously obtained by standard method. We find $\widetilde{P}_0^{cor} > \widetilde{P}_0^{stand}$, with a difference which becomes significant at $\beta = 6$, although the errors are larger. In no case however is the effect sufficient to make our low temperature results compatible with those of [5].

We do not know the reason for the unconventional behaviour of f_P observed with our algorithm. Being a sum of squares of M^{-1} matrix elements, $\widetilde{P}_0$ gets large values for configurations leading to small eigenvalues of M. As already emphasized, we do observe very large $\widetilde{P}_0$ values. However, it might happen that, in some configurations, small eigenvalues are not compensated by large ones, leading to weights $(\det M)^2$ relatively small. Such configurations are rejected (in any MC algorithm), although the product $\widetilde{P}_0 \times (\det M)^2$ may contribute the functional integral the same amount as larger weight kept configurations. (One may think of a MC computation of $\langle 1/x^2\rangle$ relative to the weight $x^2 \exp(-x^2/2)$: a correct sampling of the $x = 0$ region will require enormous statistics.) A related question raised by the vanishing of $(\det M)^2$ is that of frequent enough tunneling between regions of configuration space with opposite signs of $\det M$ [21,22]. We have computed $\det M$ for some subsets of the accepted configurations, but never found it negative. Conversely, configurations constructed by hand to yield it negative had small relative weights.

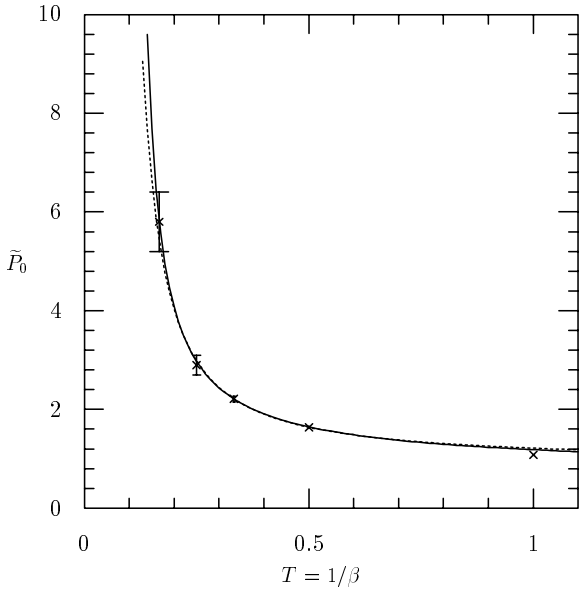

Fig. 4. $\widetilde{P}_0$ as a function of the temperature for $U = 4$ and $\mu = -0.15$. The solid curve is the fit to $\widetilde{P}_0 = b \exp\left[a/(T - T_{KT})^{1/2}\right]$, the dashed curve is the fit to $\widetilde{P}_0 = b \exp[a/T]$. The parameters are given in line 2 and 4 of Table 8.

4.3 Analysis of results in terms of a KT transition

We will now discuss the results of our numerical HMC simulations. We start with our results at $U = 4$, where we have most of the data.

We first focus on the μ-dependence of $\widetilde{P}_0$, more convenient than its filling dependence because $\langle n \rangle (\mu)$ suffers from finite size effects which are not of the same nature as those we are interested in, being important even in the non interacting case for the N_s values commonly considered. At fixed T and U, the discussion of Section 4.1 indicates that $\widetilde{P}_0$ is flat close to $\mu = 0$, and should increase with $|\mu|$ as a consequence of $T - T_{KT}(\mu, U)$ decreasing, a maximum of T_{KT} leading to a maximum of $\widetilde{P}_0$ in the same μ region. This qualitative behavior should survive in a finite, large enough box provided the function $f(x)$ of equation (40), which is proportional to $x^{-1.75}$ at large x, stays monotonic.

In order to probe such a behavior, we select out from our data of Table 5 the values of $\widetilde{P}_{0,N_s}$ obtained at the largest β (4 and 6) and $N_s = 6$ available for a sufficient range of μ values. The result is shown in Figure 3. No evidence is found for a maximum in μ within the explored β range. In this we agree with the result of [5]. Hence there is no indication that for such temperatures, the system behaves differently at and off half–filling.

We may still examine the dependence of $\widetilde{P}_{0,N_s}$ on N_s at fixed μ, to see if these data give evidence for a KT transition at $\mu \neq 0$. We therefore fix μ at -0.15, a value at which we have data in the range $1 \leq \beta \leq 6$ and for various N_s values in the 4-8 range.

In order to guess the relevant domain for the parameters b, a, T_{KT} of equations (35, 37), we first *assume* that at each β the largest N_s value available is large enough for the system to be close to its thermodynamical limit, an assumption which is verified at $\beta = 4$ as seen from our data at $N_s = 4, 6, 8$. Using the data $\widetilde{P}_0^{cor}$ of Table 7, we then perform various fits to equations (35, 37), with the results reported in Table 8. In lines 1, 3, 5, the 5 data points for β between 1 and 6 are included. Although the first fit is acceptable, we do not retain it as significant because the rather low T_{KT} value found is mainly determined by the "high" temperature points $\beta = 1$ and 2. Keeping the 4 points $\beta > 1$, we test assumption (35) with T_{KT} left free in line 2 and fixed at 0.1 [5] in line 6. From this alone, we thus find that $T_{KT} \sim 0.1$ is indeed consistent with our data (despite the fact that they do not fully agree with [5]). However, line 4 shows that the same data are equally compatible with the ansatz (35), where no KT transition is assumed to occur. The fits resulting from lines 2 and 4 are shown in Figure 4: a choice between the two curves is clearly impossible. It is no surprise in fact since, as already emphasized, no filling dependence has ever been observed in the considered data range.

We next compare the size dependence of the data with the finite size scaling expectations (40, 39). Parametrizing ξ according to (38, 36) respectively with the parameters of lines 2 and 4 of Table 8, we obtain the patterns shown in Figures 5a,b. Since both figures may be considered as suggestive of a scaling behavior, the evidence for a Kosterlitz-Thouless transition at $\mu = -0.15$ remains poor.

Similar conclusions follow from the same exercise applied to the data $\beta \leq 6$ of [5]. Clearly lower temperatures points, which we have not measured, and have not been used in the finite size analysis of [5], are necessary to establish the existence of a KT transition, and to locate it. In fact, the behaviour observed in [5] at $\beta = 10$ and $\langle n \rangle = 0.87$ as a function of N_s is close to $N_s^{1.3}$, not $N_s^{1.75}$, expected from (37, 38, 40) with $T_{KT} \sim 0.1$, and suggestive of a substantially smaller T_{KT}. Varying T_{KT} in the range 0., 0.1 we find that the data of [5] at β =8 and 10 can be included in a reasonable scaling pattern only for $0 < T_{KT} <\sim 0.04$. For illustration, we show in Figure 6a the result obtained with $T_{KT} = 0.03$. In turn, we also find that unlike the results at $\beta \leq 6$, the lowest temperature points lead to a less good agreement with the behaviour (39) as shown in Figure 6b. This is in accordance with the observation [5,6] that only at $\beta = 10$ $\widetilde{P}_0$ is larger at this filling than it is at 1/2 filling.

Hence if we take into consideration all the existing numerical information, our conclusion is: The evidence for a KT transition is weak, and if it exists T_{KT} is a few percent of k.

We did not take enough data at $U = 2$ and $U = 8$ to allow for an analysis similar to that achieved at $U = 4$. A look at Table 6 however confirms that the pair correlation increases with β at fixed $[\mu, U]$, while its values at $\mu = 0$ and -0.15 are consistent with each other at fixed $[\beta, U]$. Some information comes from comparing $\widetilde{P}_0$ at $U = 2, 4$ and 8 for $\beta = 2$ and $\mu = 0$ fixed. Its values are

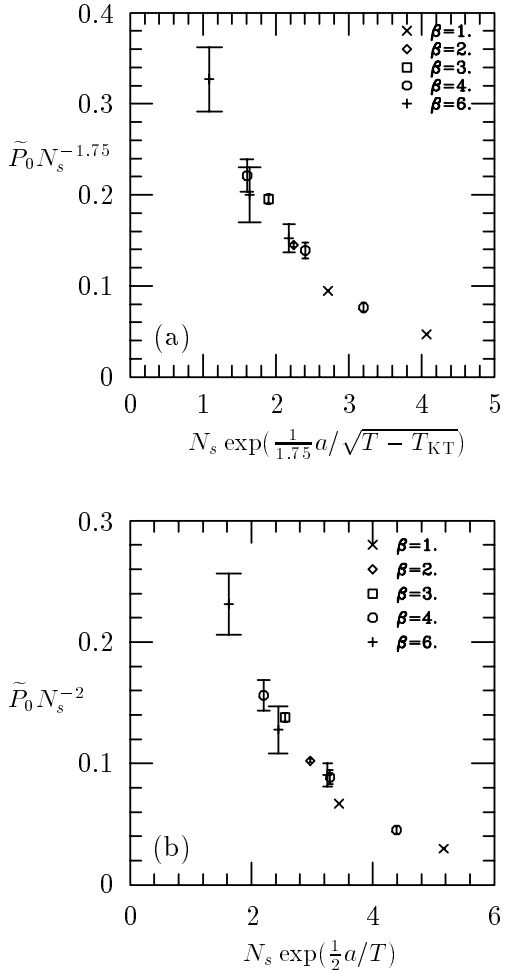

Fig. 5. Scaling of $\widetilde{P}_0$ according to equation (40) in (a) and to equation (39) in (b) with parameter a and T_{KT} from line 2 and 4 of Table 8.

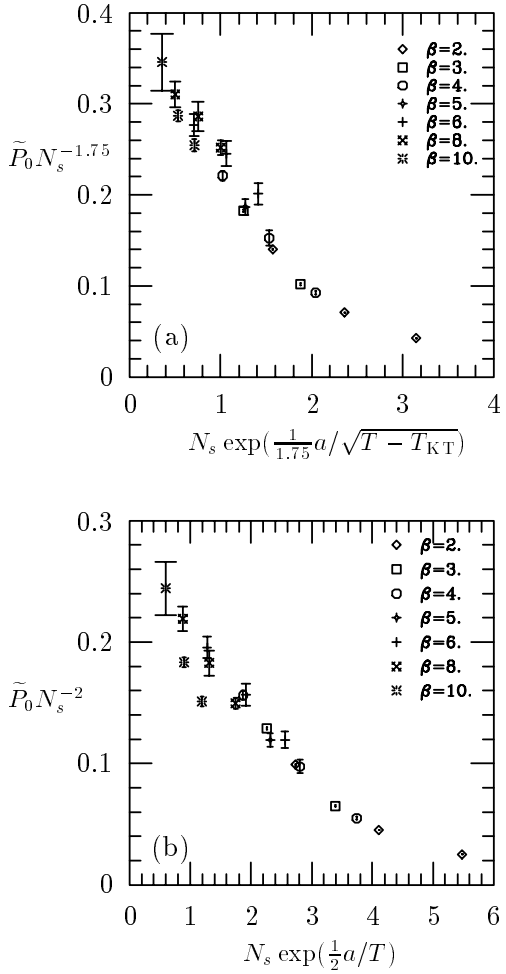

Fig. 6. Scaling of $\widetilde{P}_0$ from reference [5] according to equation (40) in (a) with $a = 1.12$ and $T_{KT} = 0.03$ and according to equation (39) in (b) with $a = 0.38$.

respectively 1.127(4), 1.63(3) and 2.2(2). It would be incorrect to directly infer from this that also the correlation length increases. In fact, as U increases at fixed temperature, more pairs are formed and this affects the normalization of the correlation function. As a measure of this normalization we take the $x = y$ (zero distance) value of the correlation of equation (6),

$$P(0) = \left\langle a_x^\dagger b_x^\dagger b_x a_x + b_x a_x a_x^\dagger b_x^\dagger \right\rangle , \qquad (44)$$

which is nothing but the average number densities of doubly occupied and empty sites, related to the single occupation probability S_1, given in Tables 5 and 6, by $P(0) = 1 - S_1$. Hence a better representative of the correlation length variations is $\widetilde{P}_0/P(0)$, and for this quantity at $\beta = 2, \mu = 0, U = 2, 4$, and 8 respectively we find 1.80(2), 2.18(4) and 2.4(2).

This leaves uncertain the guess that the correlation length is larger at $U = 8$ than it is at $U = 4$. Anyway, from the discussion for $U = 4$ we infer that no conclusion about a KT transition can be drawn without low enough temperature data, which are not available.

The above remark about the normalization of $\widetilde{P}_0$, which might be important for a discussion of the U dependence of the KT transition temperature, does not alter our previous analysis at $U = 4$ fixed because, as seen from Table 5, $P(0)$ is essentially insensitive to β, μ and N_s in the explored ranges. This is true even at temperatures as high as 1 at $U = 2$ and 4. The largest variation observed for $P(0)$ is found between $T = 0.5$ and $T = 2$, for $U = 8$, where it however does not exceed 10%. So, in the U (and μ) range considered, the pairs are very robust against temperature rises.

The independence of S_1 on the filling for fixed U in the region we investigated means that the increase in the filling goes into the formation of pairs. This is, however, also true in the free case in this region. This may be related to the fact that S_1, as well as $\widetilde{P}_0$, is an even function of μ.

Table 8. Fits of $\widetilde{P}_0$ as a function of T for $U = 4$ and $\mu = -0.15$. The point $T = 1$ is ignored in every second line. In the last two lines, $T_{\rm KT}$=0.1 is imposed.

Fitting Function	b	a	T_{KT}	N_{pts}	$\chi^2/d.o.f.$
$b\exp\left[a/\sqrt{T-T_{KT}}\right]$	0.43(4)	0.9(1)	0.04(3)	5	1.5
	0.6(1)	0.65(12)	0.085(25)	4	0.2
$b\exp\left[a/T\right]$	0.75(2)	0.37(2)		5	6.9
	0.90(5)	0.30(3)		4	0.3
$b\exp\left[a/\sqrt{T-0.1}\right]$	0.52(2)	0.69(3)	0.1	5	10.0
	0.67(5)	0.57(5)	0.1	4	0.4

5 The static, uniform susceptibility: Comparison of numerical results with hopping parameter expansion

The static, uniform spin susceptibility $\widetilde{\chi}$ in the attractive Hubbard model is known from some time [23,5] to exhibit a very fast decrease as the temperature is lowered. This feature has attracted attention, in connexion with its potential relationship with the occurrence of a spin gap [23] or of a pseudo-gap in the density of states [24], and with the physics at intermediate coupling [25,24], where a crossover from BCS to Bose-Einstein condensation is expected (for a review, see [26], a recent investigation can be found in [27]).

In this section, we bring some additional information on this behaviour of $\widetilde{\chi}$ extracted from its expansion in the hoping parameter. We first explain the method, then present and discuss the results obtained, comparing them to those of the numerical simulations. The free energy of the repulsive Hubbard model has been expanded in powers of the hopping parameter k by various authors [28–30, 3]. We start from the result of [3], where the expansion is pushed to order 5 in k^2. *Via* a particle-hole transformation on one of the two electron operators, the free energy expansion is transformed into that relevant for the Hamiltonian in the attractive case equation (1). For arbitrary values of β^{-1}, μ and h respectively of the temperature, chemical potential and external magnetic field, we end up with the following truncated expansion (F is the negative of β times the free energy density)

$$F(\beta,U,\mu,h) \equiv \frac{1}{V}\ln Z + \mathcal{O}(k^{12}) = \log z + \sum_{\kappa=1}^{5}\sum_{\{R\}} \frac{v^{2\kappa}}{(\beta U)^i} x^{i_\mu} y^{i_h} w^{i_w} C_{\kappa;\{R\}}, \tag{45}$$

where

$$x = e^{\beta\mu}, y = e^{\beta h}, w = \exp\left[-\frac{\beta U}{2}\right]$$
$$v = \frac{\beta k}{z}$$
$$z = 1 + xw\,(y + 1/y) + x^2, \tag{46}$$

and $\{R\}$ represents the set of integers $\{i, i_\mu, i_h, i_w\}$.

Table 9. The ratios A_κ/A_0 of the expansion of $\widetilde{\chi}$ in powers of k^2 for $U = 4$, $\mu = 0$, $\beta = 1$ and 2.

κ	0	1	2	3	4	5
$\beta = 1$	1.0	0.580	−0.725	0.372	0.156	−0.497
$\beta = 2$	1.0	5.65	2.91	−17.6	−0.404	62.5

The symbol $C_{\kappa,\{R\}}$ represents the 3836 non zero coefficients provided in [3], labeled by the order κ in k^2 and the associated set $\{R\}$. By differentiation with respect to μ and h, one obtains similar series (here taken at zero magnetic field) for the filling density, the static uniform charge density correlation and the static uniform spin susceptibility. We focus on the latter, and study the truncated series

$$\frac{1}{\beta}\widetilde{\chi}(q=0) = \left(y\frac{d}{dy}\right)^2 F \equiv \sum_{\kappa=0}^{5} A_\kappa k^{2\kappa}. \tag{47}$$

The coefficients A_κ follow from the expansion (45) of F. Although it is not strictly speaking a high temperature series, but a series in (βk^2) with β-dependent coefficients, extracting information from such short expansions at low temperature is notoriously difficult [31].

An idea of the problem at hand is given by the following examples. We take $U = 4$, $\mu = 0$ and compute the coefficients A_κ for $\beta = 1$ and 2. Their numerical ratios to A_0 are shown in Table 9.

One observes a quite discouraging pattern of orders of magnitude and signs (remember we want to evaluate $\widetilde{\chi}$ at $k = 1$). We tried to understand what happens by starting from the free case $U = 0$, at $\mu = 0$. The exact susceptibility is given by

$$\widetilde{\chi} = \beta \int_0^\pi \frac{dp_1 dp_2}{\pi^2} \frac{1}{1+\cosh(2k\beta\delta_p)} \tag{48}$$

with

$$\delta_p = -(\cos p_1 + \cos p_2). \tag{49}$$

Its expansion in $(\beta k)^2$ to 5th order is found to be

$$\frac{2\widetilde{\chi}}{\beta} = 1 - (\beta k)^2 + \frac{3}{2}(\beta k)^4 - \frac{85}{36}(\beta k)^6 + \frac{1085}{288}(\beta k)^8 - \frac{4837}{800}(\beta k)^{10}. \tag{50}$$

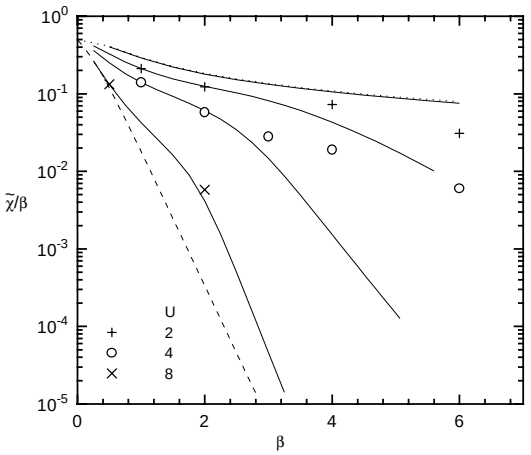

Fig. 7. $\widetilde{\chi}/\beta$ as a function of β for different values of the coupling U at $\mu = 0$. See description in the text.

The signs alternate, but again the size of the coefficients in k^2 increases fast, the more so the temperature is lowered. The origin of this blow up is clear from expression (48). Rewriting it as

$$\frac{\widetilde{\chi}}{\beta} = \int_0^2 d\delta \rho(\delta) \frac{1}{1+\cosh(2k\beta\delta)} \tag{51}$$

where $\rho(\delta)$ represents the density of states, and recalling that ρ has only a logarithmic (van Hove) singularity at $\delta = 0$, all singularities of $\widetilde{\chi}$ in k at finite distance are end point ($\delta = 2$) singularities. They are located at $\cosh(4k\beta) = -1$, and the closest one, which fixes the radius of convergence, is at $(\beta k)^2 = -\pi^2/16$. Hence the alternate signs in the above series and also the fact that $\pi^2/16$ times the ratio $|A_5/A_4|$ is very close to 1 (namely 0.990). Finally, we note from the above integral that the most singular part of $\widetilde{\chi}/\beta$ is proportional to $\tanh(2\beta k)/(\beta k)$. This leads us to perform the change of variable $\beta k \to u$ defined by

$$u = \tanh(2\beta k)/(\beta k) - 2, \tag{52}$$

and to re-expand $\widetilde{\chi}/\beta$ in powers of u. We find

$$\frac{2\widetilde{\chi}}{\beta} = 1 + \frac{3u}{8} - \frac{9u^2}{640} + \frac{246u^3}{51469} - \frac{4096u^4}{2238401} + \frac{30034u^5}{40581943} + \cdots \tag{53}$$

that is

$$\frac{2\widetilde{\chi}}{\beta} \simeq 1.0 + 0.375u - 1.41 \times 10^{-2}u^2 + 4.78 \times 10^{-3}u^3 - 1.83 \times 10^{-3}u^4 + 7.40 \times 10^{-4}u^5. \tag{54}$$

The interval $\beta k \geq 0$ is mapped onto $-2 \leq u \leq 0$, and low temperatures mean $u \sim -2$. Clearly this series in u looks much more tractable than the original one. Indeed, actual comparison of Padé approximants of (54) with the exact result (48) shows that, up to $\beta \sim 10$, the latter can be approached with an accuracy better than 5%, an achievement not expected from the series (50)!

In the absence of any information on the analytic structure of $\widetilde{\chi}$ in k as the interaction is turned on, we decided to perform the same change of variable (52) in all cases and constructed the Padé approximants to the series in u. We observe that the [2,3] and [3,2] approximants systematically lead to very similar results. Our results for $\mu = 0$ are collected in Figure 7, and compared with those of the numerical simulation, as obtained with the largest lattices which were simulated for each set of β, U values. We now describe and comment this figure.

The upper (dotted) curve is the exact result in the free case $U = 0$. The four continuous lines are the [2,3] Padé results for respectively $U = 0.1, 2, 4, 8$, from top to bottom. The lower (dashed) line is the "atomic" limit ($k = 0$) drawn for $U = 8$. The statistical errors are smaller than the size of the symbols representing our numerical results for the largest available values of N_s, N_t. When comparisons can be made, our results are in general agreement with published data [23,5,27].

The $U = 0.1$ curve is used as an overall check that the whole series constructed from [3] is correctly implemented and that the change of variable and Padé reconstruction work close to the free case. For $U = 2$, excellent agreement between series and data is obtained at $\beta = 1$ and 2. The figure suggests that at $\beta = 3$, the series still gives a reasonable answer, although lower than the true one by probably 10 to 15%. A similar departure shows up above $\beta = 2$ at $U = 4$, and, say, $\beta = 1.5$ at $U = 8$. Hence the overall pattern is that our treatment of the series gives good results at β values below a maximum which decreases as U increases. Above this maximum, the Padé approximant drops down rapidly the more so when U is large. It is interesting to discuss this latter feature. Consider again the case $U = 8$. The dashed line ($k = 0$) is the curve

$$\frac{\widetilde{\chi}}{\beta} = \frac{w}{1+w}\ ,\ w = \exp[-\beta U/2], \tag{55}$$

drawn for $U = 8$, thus falling down like $\exp[-4\beta]$. One observes that the Padé result at $U = 8$ drops down roughly parallel to it above $\beta = 2$.

Inspection of the series for $\widetilde{\chi}$ reveals that all (known) terms of its expansion in k^2 contain at least one power of w as a factor. So any truncation unavoidably leads to an exponential fall off in β at fixed U, the more so when U is large. This is what we observe with the series at hand, while the numerical simulation indicates that, although $\widetilde{\chi}$ actually decreases as β increases, it does so at a *much slower* rate than naively expected. In other words, there are collective effects which rather tend to maintain a sizable susceptibility, even though low temperature or/and large U favor the formation of local pairs, which contribute zero to the total spin. We note that, as already mentioned in the previous section, the probability for single occupation, S_1 (as given in Tabs. 5 and 6) and thus the average local pair number $\langle n/2 \rangle - S_1/2$, depends weakly upon temperature. Hence the decrease of $\widetilde{\chi}$ with T is *not* a consequence (only) of pair formation at fixed U and $\langle n \rangle$.

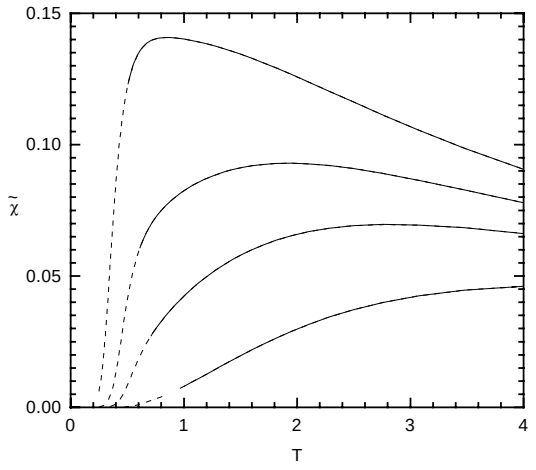

Fig. 8. $\widetilde{\chi}$ as a function of T for different values of the coupling U at $\mu = 0$. From top to bottom $U = 4, 6, 8$ and 12. See description in the text.

Its sensitivity to U also is strong compared to that of S_1. These questions are of interest in connection with the kind of regime (BCS-like or pair condensation) eventually leading to a superconducting transition [5,23,27].

Our results show that, unlike popular approximations such as RPA or T-matrix treatment, the series expansion in k^2 can be continued successfully down to fairly small T values even at large coupling. In order to further illustrate this point, we present our predictions for $\widetilde{\chi}$ as a function of T for $U = 4$, 6, 8 and 12, at half filling ($\langle n \rangle = 1$), in Figure 6. These predictions appear as solid lines when our calculation is accurate (the minimum T's of the solid lines are conservative guesses). We point out that by themselves these results clearly expose the main features of physical interest, namely the existence of a crossover from a smooth regime at high T to a rapid fall off below a U dependent T value. Furthermore, we observe that these $\widetilde{\chi}$ values are quantitatively very close to that of [27] obtained numerically at the same U values, but for $\langle n \rangle = 0.8$. This enforces our general statement that there is no evidence for any substantial dependence on filling.

6 Summary and conclusion

Motivated by the interest for strongly interacting systems of electrons in the context of high T_c materials, we have performed an investigation of the attractive Hubbard model.

Based on the hybrid Monte-Carlo method to simulate the path integral representation of the partition function, a numerical study provided us with estimates of the static zero-momentum pair correlation $\widetilde{P}_0$ and spin susceptibility $\widetilde{\chi}$. The exploration covered the ranges [0.5, 6.0] for the inverse temperature β and [2.0, 8.0] for the interaction strength U in units of the hopping parameter k. At $U = 4$ we investigated in detail the dependence on the chemical potential in order to study the sensitivity of these physical quantities to band filling, in the neighbourhood of half filling. We also performed an analytical investigation of the susceptibility, based on its expansion in k^2 to order 5 derived from the results of [3] and on a specific Padé resummation technique inspired by the free case. We showed that this method yields very good results for $\beta \lesssim 1$ at any U, and $\beta \lesssim 2$ for $U \lesssim 4$.

In the numerical approach, the cost in computer time leads to the consideration of rather small lattices only, and also limits the number of time slices involved. The limitation of the analytical approach is obviously due the truncation of the k^2 expansion. Furthermore this expansion is not available for the pair correlation. But it yields estimates of $\widetilde{\chi}$ directly in the thermodynamical limit, so that the two approaches are complementary and their comparison brings valuable information. Whenever it was possible, we also compared our numerical data with those of previous investigations [5,4,27] performed using Quantum Monte-Carlo. The overall agreement is good for most quantities but we found significant and unresolved discrepancies for $\widetilde{P}_0$ at our lowest T values.

Using pair correlations, the main question addressed was that of the existence and location T_{KT} of a Kosterlitz-Thouless superconducting transition, the only possible transition at finite temperature away from half filling. Our results show very weak dependence on μ, hardly distinguishing half filling from other values of band filling in the range between 0.8 and 1.0. In the temperature range $\beta \leq 6$, fits or finite size analysis relevant to a KT transition are consistent with a transition temperature which may reach ~ 0.1, the value proposed in [5], with a weak dependence on filling, if any. However, they are compatible as well with lower T_{KT} values, and even with no finite temperature transition at all, which must be the case at 1/2 filling. Including lower temperature data ($\beta = 8$ and 10 at $\langle n \rangle = 0.87$ [5]) in the analysis, we then showed that while they are incompatible with $T_{KT} \sim 0.1$, they favour a KT transition below ~ 0.04. Our analysis also shows that a better understanding of the model requires a systematic comparison of data taken at and off half-filling, at temperatures below $\sim 1/8$. In the mean time, any conclusion on how T_{KT} depends on U seems premature.

Our study of the magnetic susceptibility shows that it depends very weakly on the band filling, but decreases rapidly with increasing U and/or decreasing temperature, in agreement with previous investigations [23,5,27]. Increasing U favors S-wave pair formation, reducing the probability S_1 of sites occupied by a single electron responding to a magnetic field. This explains the simultaneous decrease of $\widetilde{\chi}$ and S_1 at fixed temperature. But at fixed U, we observe that S_1 stays approximately constant in the low temperature range whereas $\widetilde{\chi}$ falls steeply. This casts some doubt on the existence of a tight connection between the static uniform susceptibility and pair formation as the expected transition is approached as claimed in [27].

We would like to thank Thierry Jolicœur for many interesting discussions and for his careful reading of our manuscript. We further thank J. Oitmaa for providing us with the latest results

on the series expansion in suitable form. Two of us (B.P. and J.S.) are grateful to the Deutsche Forschungsgemeinschaft for support. Calculations were performed at HLRZ (Jülich) and CEA (Grenoble).

References

1. J. Hubbard, Proc. R. Soc. London A **276**, 283 (1963); A **281**, 401 (1964).
2. J.M. Kosterlitz, D.J. Thouless, J. Phys. C **6**, 1181 (1973).
3. J. Oitmaa, J.A. Henderson, Aust. J. Phys. **46**, 613 (1993).
4. R.T. Scalettar, E.Y. Loh, J.E. Gubernatis, A. Moreo, S.R. White, D.J. Scalapino, R.L. Sugar, E. Dagotto, Phys. Rev. Lett. **62**, 1407 (1989).
5. A. Moreo, D.J. Scalapino, Phys. Rev. Lett. **66**, 946 (1991); A. Moreo, D.J. Scalapino, S.R. White, Phys. Rev. B **45**, 7544 (1992).
6. We thank A. Moreo for providing us with some of these data and for confirming that only at T/k as low as 0.1 is the pairing function enhanced away from half-filling as compared to the half filled case.
7. C.N. Yang, S.C. Zhang, Mod. Phys. Lett. B **4**, 759 (1990); S.C. Zhang, Phys. Rev. Lett. **65**, 120 (1990).
8. S. Duane, Nucl. Phys. B **257**, 652 (1985); S. Duane, J. Kogut, Phys. Rev. Lett. **55**, 2774 (1985); G. Batrouni, G.R. Katz, A.S. Kronfeld, G.P. Lepage, B. Svetitsky, K.G. Wilson, Phys. Rev D **32**, 2736 (1985).
9. R.T. Scalettar, D.J. Scalapino, R.L. Sugar, Phys. Rev. B **34**, 7911 (1986).
10. R.T. Scalettar, D.J. Scalapino, R.L. Sugar, D. Toussaint, Phys. Rev. B **36**, 8632 (1987).
11. M. Creutz, Phys. Rev D **38**, 1228 (1988).
12. R. Gupta, G.W. Kilcup, S.R. Sharpe, Phys. Rev D **38**, 1278 (1988).
13. S. Gupta, A. Irbäck, F. Karsch, B. Petersson, Phys. Lett. B **242**, 437 (1990).
14. R.M. Fye, Phys. Rev. B **33**, 6271 (1986); R.M. Fye, R.T. Scalettar, Phys. Rev. B **36**, 3833 (1987).
15. S.R. White, D.J. Scalapino, R.L. Sugar, E.Y. Loh, J.E. Gubernatis, R.T. Scalettar, Phys. Rev. B **40**, 506 (1989).
16. P.B. Mackenzie, Phys. Lett. B **226**, 369 (1989).
17. D. Weingarten, Nucl. Phys. B (Proc. Suppl.) **9**, 447 (1989).
18. G.H. Golub, C.F. van Loan, *Matrix Computations* (Johns Hopkins University Press, Baltimore Maryland, 1983).
19. P.J.H. Denteneer, An Guozhong, J.M.J. van Leuwen, Europhys. Lett. **16**, 5 (1991); **16**, 509 (1991).
20. J.P. Bouchaud, A. Georges, Phys. Rep. **195**, 128 (1990).
21. J.E. Hirsch, Phys. Rev. B **31**, 4403 (1985).
22. S.R. White, J.W. Wilkins, Phys. Rev. B **37**, 5024 (1988); S.R. White, R.L. Sugar, R.T. Scalettar, Phys. Rev. B **38**, 11665 (1988).
23. M. Randeria, N. Trivedi, A. Moreo, R.T. Scalettar, Phys. Rev. Lett. **69**, 2001 (1992).
24. N. Trivedi, M. Randeria, Phys. Rev. Lett. **75**, 312 (1995).
25. C. Sa de Melo, M. Randeria, J.R. Engelbrecht, Phys. Rev. Lett. **71**, 3202 (1993).
26. M. Randeria, in *Bose-Einstein Condensation* (Cambridge University Press 1995) and references therein.
27. J.M. Singer, M.H. Pedersen, T. Schneider, H. Beck, H.G. Matuttis, Phys. Rev. B **54**, 1286 (1996).
28. K.K. Pan, Y.L. Wang, Phys. Rev. B **43**, 3706 (1991); J. Appl. Phys. **69**, 4656 (1991), references to earlier work therein.
29. D.F.B. ten Hopf, J.M.S. van Leeuwen, Phys. Rev. B **46**, 6313 (1992).
30. J.A. Henderson, J. Oitmaa, M.C.B. Ashley, Phys. Rev. B **46**, 6328 (1992).
31. An attempt to overcome this problem is proposed in: D.F.B. ten Haaf, P.W. Brouwer, P.J.H. Denteneer, J.M.J. van Leuwen, Phys. Rev. B **51**, 353 (1995), for the repulsive Hubbard model. There use is made of the hole filling density being small at large $-U$ close to half filling for the electrons. In the attractive case, the corresponding small parameter would be the single occupation density.